Inorg. Chem. **2002**, *41*, 5024–5033

A Ligand-Field Analysis of the trensal (H_3trensal = 2,2′,2″-Tris(salicylideneimino)triethylamine) Ligand. An Application of the Angular Overlap Model to Lanthanides

Bernadine M. Flanagan,[†] Paul V. Bernhardt,[†] Elmars R. Krausz,[‡] Stefan R. Lüthi,[†] and Mark J. Riley*,[†]

Department of Chemistry, University of Queensland, St. Lucia 4072, Australia, and Research School of Chemistry, Australian National University, Canberra 0200, Australia

Received December 12, 2001

The spectral and geometric trends of Ln(trensal) complexes (H_3trensal = 2,2′,2″-tris(salicylideneimino)triethylamine) along the lanthanide series are analyzed. Low-temperature polarized absorption and luminescence spectra are reported for nine of the complexes with transitions suitable for analysis. Both the angular and radial geometry variations as a function of the lanthanide ion are quantified. The structural parameters are related to the trend in the ligand field found from an analysis of the f–f transitions. The ligand-field analysis is fitted globally across the whole series accounting for the contraction of the f orbitals as a function of atomic number. This study establishes the utility of describing the ligand field of f electrons within the one-electron operator approach of the angular overlap model.

Introduction

There have been few comparative ligand-field analyses along the lanthanide series. Most commonly these have focused on Ln(III)-doped ionic lattices such as $LiYF_4$,[1] $YAlO_3$,[2] YAG,[3] Cs_2NaYCl_6,[4] $LaCl_3$,[5] and LaF_3[6] where the guest ion substitutes for either yttrium(III) or lanthanum(III). These studies have the disadvantage that the trends in the ligand-field parameters are related to the *inferred* geometry changes based on the site symmetry of the host and the expected change in ionic radii of the guest ions. Alternatively, in neat crystal systems such as $Na_3[Ln(oda)_3]\cdot 2NaClO_4\cdot 6H_2O$ (Ln = Ce−Yb; oda = oxydiacetate),[7] although the isomorphous nature of the series has been established, a fully refined crystal structure of each member is lacking; thus, the local coordination environment (bond lengths and angles) is not known.

Recently the relationship between two different descriptions of the ligand field for the Er(trensal) (H_3trensal = 2,2′,2″-tris(salicylideneimino)triethylamine) complex was investigated.[8] The angular overlap model (AOM) σ- and π-bonding parameters were related to the symmetry-determined "crystal-field" coefficients of the spherical harmonic expansion of the ligand field. Reasonably good agreement was found between these two approaches, and it was proposed that the AOM may prove useful as a "first guess" of the ligand fields of lanthanide complexes of lower symmetry. In low-symmetry complexes, there are many crystal-field parameters and the parameter space can often have multiple solutions when the difference between observed and calculated energy levels is minimized. It is often unclear which parameter set best describes the ligand field. In the present work, we treat a complete series of Ln(III) complexes (except for radioactive Pm(III)) where there are small and systematic changes in the ligand geometry about the metal ion. We also expect small and systematic changes in the ligand field so that the best fit for a particular complex must also fit the trend across the series.

* Author to whom correspondence should be addressed. E-mail: riley@chemistry.uq.edu.au.
[†] University of Queensland.
[‡] Australian National University.

(1) Jayasankar, C. K.; Reid, M. F.; Richardson, F. S. *Phys. Status Solidi B* **1989**, *155*, 559.
(2) Deb, K. K. *J. Phys. Chem. Solids* **1982**, *43*, 189.
(3) Morrison, C. A.; Wortman, D. E.; Karayianis, N. *J. Phys. C* **1976**, *9*, L191.
(4) Tanner, P. A.; Kumar, V. V. R. K.; Jayasankar, C. K.; Reid, M. F. *J. Alloys Compd.* **1994**, *215*, 349.
(5) Jayasankar, C. K.; Richardson, F. S.; Reid, M. F. *J. Less-Common Met.* **1989**, *148*, 289.
(6) Carnell, W. T.; Goodman, G. L.; Rajnak, K.; Rana, R. S. *J. Chem. Phys.* **1989**, *90*, 3443.
(7) Hopkins, T. A.; Metcalf, D. H.; Richardson, F. S. *Inorg. Chem.* **1998**, *37*, 1401.
(8) Flanagan, B. M.; Bernhardt, P. V.; Lüthi, S. R.; Krausz, E. R.; Riley, M. J. *Inorg. Chem.* **2001**, *40*, 5401.

10.1021/ic011276q CCC: $22.00
Published on Web 09/06/2002

The heptadentate tripodal ligand "trensal" forms stable complexes with lanthanide(3+) ions. This ligand has the important advantage that it forms a complete isomorphous and isostructural series with all lanthanide complexes. A three-dimensional structure determination leaves no doubt of the geometry of the lanthanide complex unlike a doped crystal system. An analysis of the Er(trensal) complex has shown that this ligand has one of the largest ligand fields observed for a lanthanide complex, 3-fold greater than that of the simple halide $LaCl_3$ host, for example.[8] The large ligand field and complete structural data over the whole isomorphous series allow us to examine a global fit of crystal-field parameters and to relate the AOM parameters to the observed small structural changes. We analyze the trend in terms of the one-electron-operator, additive ligand-field approach of the AOM.

Experimental Section

Synthesis and Structure. Details of the synthesis[9] and structural characterization[10] of these compounds have been described previously. It is possible to crystallize all compounds in the trigonal space group $P\bar{3}c1$. Care must be taken as it has been found[11,12] that polymorphic (Ln = Pr, Nd, Eu, Gd, Tb) trensal compounds are known which include solvent molecules in the structure, which crystallizes in the $P\bar{3}$ space group under different synthetic conditions. Our compounds are all exclusive of solvent and have the Ln(III) ions lying on a C_3 site of the $P\bar{3}c1$ space group. Typically the crystals have a needlelike habit with the crystallographic *c* axis coinciding with the long crystal axis.

Figure 1 shows the Er(trensal) complex. The heptadentate trensal ligand binds in a N_4O_3 fashion, resulting in a trigonally capped distorted octahedron, with the C_3 axis passing through the Ln(III) ion and the apical tertiary amine (N1). The 3-fold symmetry relates the N2 imine and O1 atoms. These three independent metal−ligand bond lengths for all Ln(trensal) complexes (barring Pm) are given in Table 1. Also included are the structural parameters for the trensal ligand complexed to Cr(III) for comparison. With the smaller transition-metal ions, the apical N1 of the trensal ligand is not bound and the coordination is that of a distorted octahedron.

Spectroscopic Investigations. Polarized absorption spectra were recorded at 10 K on a single-beam absorption instrument as described previously.[8,13] The near-IR absorption spectra were collected using a liquid-N_2-cooled InSb detector with a 600 lines/mm grating blazed at 1600 nm, while measurements of the visible spectra were done using an S-20 photomultiplier tube with a 1200 lines/mm grating blazed at 500 nm. Luminescence spectra were obtained using the 356.4 and 350.7 nm lines of a Kr^+ ion laser as the excitation source. For absorption and luminescence experiments at 10 K, the samples were cooled with a helium flow-tube cryostat. Raman measurements were made on powdered samples at room temperature on a Perkin-Elmer FT-Raman 2000 instrument.

Computational Procedures. We used the Reid suite of programs[14] to calculate the f^n multiplet energies. The large ligand field

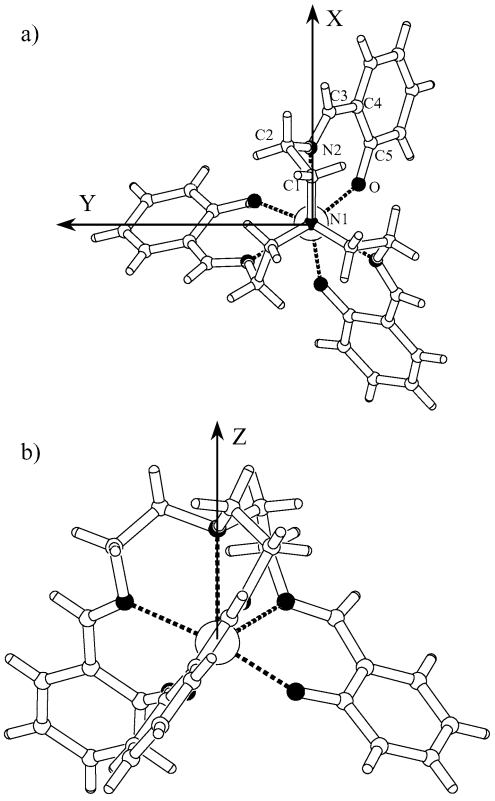

Figure 1. Molecular structure of Er(trensal). (a) Viewed down the *c* axis, showing the atom labels. Coordinating atoms are shown in black. (b) Edge-on view to the N2−Er−O1 bidentate ring showing the angle that it makes with the trigonal axis.

encountered for the trensal ligand[8] implies extensive mixing of the atomic levels, and care must be taken to use an adequate basis. We used the full basis for $f^{1-3(11-13)}$ and the truncated bases of 754 for f^5, 477 for f^6, 789 for f^8, 594 for f^9, and 559 for f^{10}. In all cases the truncated atomic levels were >40000 cm^{-1} above the ground state.

Results

Experimental Spectra. A representative overview of the absorption spectrum of Sm(trensal) is shown in Figure 2 for a crystal of ~200 × 200 μm. The spectrum is typical of those measured across the lanthanide series. The noise at 5300 and 7200 cm^{-1} is due to the absorption of water overtone bands. The onset of ligand absorption occurs at ~25000 cm^{-1}. Particularly intense transitions have the potential to be saturated at an absorbance >1.0, due to the small crystal size. This is dependent on the optical quality of the crystal; with some samples it was possible to measure an absorbance of up to 2.5.

A representative luminescence spectrum of Sm(trensal) is shown in Figure 3. As observed previously for Er(trensal),[8] efficient energy transfer from the ligand-based absorption to the metal-based luminescence occurs. Figure 3 also shows that luminescence occurs at room temperature. This is unusual for a lanthanide complexed to an organic ligand as the high-energy vibrations of the ligand are usually efficient in nonradiative relaxation processes. The luminescent hot bands due to the thermal population of higher levels of the excited-state multiplet are indicated (by an H). The observed

(9) Bernhardt, P. V.; Flanagan, B. M.; Riley, M. J. *Aust. J. Chem.* **2000**, *53*, 229.
(10) Bernhardt, P. V.; Flanagan, B. M.; Riley, M. J. *Aust. J. Chem.* **2001**, *54*, 229.
(11) Kanesato, M.; Yokoyama, T.; Itabashi, O.; Suzuki, T. M.; Shiro, M. *Bull. Chem. Soc. Jpn.* **1996**, *69*, 1297.
(12) Kanesato, M.; Yokoyama, T. *Chem. Lett.* **1999**, 137.
(13) Krausz, E. R. *Aust. J. Chem.* **1993**, *46*, 1041.
(14) Reid, M. F. *J. Chem. Phys.* **1987**, *87*, 2875.

Table 1. Structural Parameters of the Ln(trensal) Complexes

	Ce	Pr	Nd	Sm	Eu	Gd	Tb	Dy	Ho	Er	Tm	Yb	Lu	Cr
M−N1/Å	2.836	2.816	2.796	2.780	2.756	2.705	2.739	2.746	2.713	2.713	2.698	2.693	2.697	3.244
M−N2/Å	2.607	2.583	2.576	2.539	2.533	2.508	2.491	2.476	2.450	2.460	2.444	2.428	2.424	2.102
M−O/Å	2.287	2.280	2.273	2.246	2.237	2.240	2.222	2.202	2.194	2.186	2.172	2.161	2.156	1.940
θ_{N2}/deg	64.54	65.07	65.43	65.80	65.60	66.30	66.14	66.34	66.37	66.51	66.63	67.20	66.77	59.2
θ_{O}/deg	118.5	119.2	119.6	120.0	120.2	120.9	121.2	121.4	122.0	122.1	121.8	122.2	122.9	125.2
ϕ_{O}/deg	46.94	47.30	47.59	49.49	49.84	48.92	50.33	51.07	51.64	51.64	52.36	52.29	52.59	63.8
ψ_{N2}/deg	31.55	31.07	33.88	35.76	34.44	33.77	36.07	37.67	37.07	36.57	37.05	37.62	37.05	43.34
ψ_{O}/deg	62.10	60.90	61.47	63.27	62.30	61.87	61.87	62.88	62.58	63.00	64.07	64.21	62.99	47.64

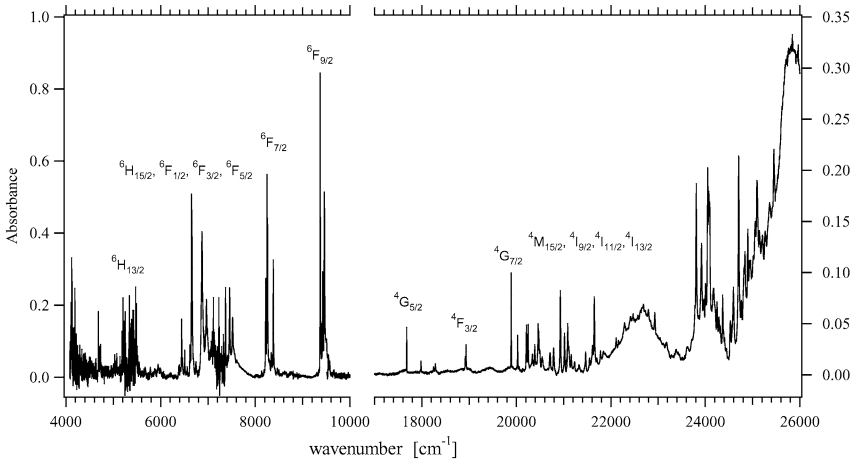

Figure 2. Overview absorption spectrum of Sm(trensal) at 10 K in σ polarization.

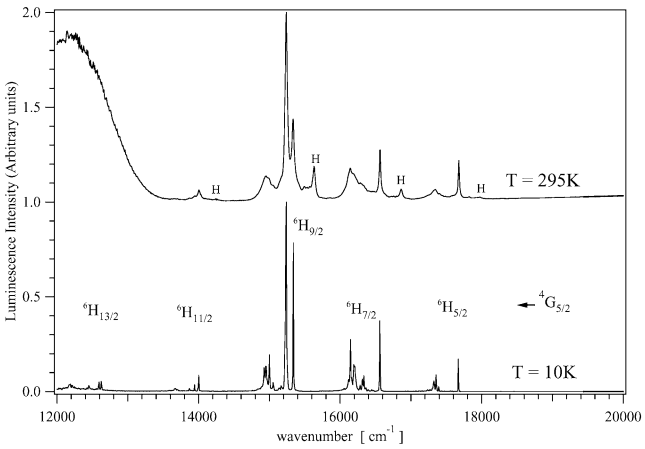

Figure 3. Overview luminescence spectrum of Sm(trensal) at 10 K and room temperature. H denotes hot bands present in the room-temperature spectrum only.

f−f transition energies of Ln(trensal) and their assignments are given in Table 2.

Spectra were not obtained for Ln(trensal) where Ln = Ce, Gd, or Yb. The f^7 Gd complex does not have absorption bands in the 0−25000 cm^{-1} optical window of the ligand, while the small number of transitions in the f^1 Ce and f^{13} Yb complexes, compared to the number of fitting parameters required for the C_3 ligand field, precludes an analysis.

Assignment of the Spectra. In C_3 symmetry the energy levels of the Ln(trensal) complexes are split into two sets of irreducible representations. For even-electron systems these are the singly and doubly degenerate irreducible representations Γ_1 and (Γ_2, Γ_3), respectively, using Bethe Γ notation.[15] For odd-electron systems they are the Kramers doublets (Γ_4, Γ_5) and (Γ_6, Γ_6). In what follows we will refer to these as Γ_1, $\Gamma_{2,3}$ and $\Gamma_{4,5}$, $2\Gamma_6$ for even- and odd-electron cases, respectively, with the understanding that $\Gamma_{2,3}$ is doubly degenerate and that $\Gamma_{4,5}$ and $2\Gamma_6$ are each Kramers doublets. The absorption spectra will show polarization anisotropy parallel and perpendicular to the crystallographic *c* axis, and the selection rules for transitions between these two sets of states for electric-dipole-allowed transitions are given in Table 3 for both even- and odd-electron cases. For all even-electron Ln(trensal) complexes the ground state is Γ_1, while for all odd-electron complexes the ground state is $\Gamma_{4,5}$. The spectroscopy of the even-electron systems allows one to determine whether the C_3 symmetry of the complex in the room-temperature crystal structure is maintained at 10 K, as the $\Gamma_{2,3}$ state will split in lower symmetry while states of other irreducible representations will not. In no cases was a splitting observed that could be attributed to a lowering of the C_3 symmetry of the room-temperature structure. Figures 4 and 5 show a more detailed representative spectrum in the IR and visible regions, this time for Nd(trensal). Here the intensities of the calculated peaks have been obtained using the intensity parameters found for the Er(trensal) complex without change.[8] While some polarization information is evident, it is not clear-cut as implied by the selection rules in Table 3, which may indicate that a phase change occurs at low temperature. Some complexes (Tb and Ho) have low-energy excited states (<10 cm^{-1}) that could remove some of the ideal polarization behavior. There are some transitions which have appreciable magnetic-dipole-allowed intensities (i.e., $^7F_0 \rightarrow {}^5D_0$ in Eu(III)), and in others the true relative

(15) Koster, G. F.; Dimmock, J. O.; Wheeler, R. G.; Statz, H. *Properties of the Thirty-Two Point Groups*; MIT Press: Cambridge, MA, 1963.

Table 2. Observed Energy Levels[a]

multiplet[b]		energy obsd	multiplet[b]		energy obsd	multiplet[b]		energy obsd	multiplet[b]		energy obsd
					Pr(trensal)						
$^3H_4$	Γ_1	0	$^3F_3$	Γ_1	6644	$^1D_2$	$\Gamma_{2,3}$	16552	$^3P_1$	Γ_1	21151
$^3H_6$	$\Gamma_{2,3}$	4942		$\Gamma_{2,3}$	6742		Γ_1	17014		$\Gamma_{2,3}$	21343
	$\Gamma_{2,3}$	5001		Γ_1	6847		$\Gamma_{2,3}$	17353	$^1I_6$	Γ_1	21792
	Γ_1	5178		$\Gamma_{2,3}$	6919	$^3P_0$	Γ_1	20696		$\Gamma_{2,3}$	22011
$^3F_2$	$\Gamma_{2,3}$	5494	$^3F_4$	$\Gamma_{2,3}$	7250	$^1I_6$	Γ_1	20899	$^3P_2$	$\Gamma_{2,3}$	22464
	$\Gamma_{2,3}$	5581		$\Gamma_{2,3}$	7533		$\Gamma_{2,3}$	20939			
	Γ_1	5750	$^1G_4$	Γ_1	9876						
				$\Gamma_{2,3}$	10001						
					Nd(trensal)						
$^4I_{9/2}$	$\Gamma_{4,5}$	0	$^4S_{3/2}$	$\Gamma_{4,5}$	13581	$^4G_{7/2}$	$\Gamma_{4,5}$	17303	$^2G_{9/2}$	$2\Gamma_6$	20750
$^4I_{15/2}$	$\Gamma_{4,5}$	5668	$^4F_{7/2}$	$\Gamma_{4,5}$	13622		$\Gamma_{4,5}$	17352		$\Gamma_{4,5}$	20818
	$2\Gamma_6$	5762		$\Gamma_{4,5}$	13725		$2\Gamma_6$	17398		$2\Gamma_6$	20887
	$2\Gamma_6$	6145	$^4F_{9/2}$	$2\Gamma_6$	14661	$^4G_{5/2}$	$\Gamma_{4,5}$	17600		$2\Gamma_6$	21022
$^4F_{3/2}$	$2\Gamma_6$	11412		$\Gamma_{4,5}$	14685	$^4G_{7/2}$	$\Gamma_{4,5}$	18749	$^4G_{9/2}$	$\Gamma_{4,5}$	21137
	$\Gamma_{4,5}$	11566		$\Gamma_{4,5}$	14807		$\Gamma_{4,5}$	18896		$\Gamma_{4,5}$	21182
$^4F_{5/2}$	$\Gamma_{4,5}$	12384		$2\Gamma_6$	14933		$\Gamma_{4,5}$	19028	$^4G_{11/2}$	$2\Gamma_6$	21257
$^2H_{9/2}$	$2\Gamma_6$	12484		$\Gamma_{4,5}$	14994	$^4G_{9/2}$	$2\Gamma_6$	19287	$^2K_{15/2}$	$\Gamma_{4,5}$	21490
$^4F_{5/2}$	$2\Gamma_6$	12492	$^2H_{11/2}$	$\Gamma_{4,5}$	15833[c]		$\Gamma_{4,5}$	19429		$2\Gamma_6$	21544
	$\Gamma_{4,5}$	12642		$\Gamma_{4,5}$	15902[c]	$^2K_{13/2}$	$2\Gamma_6$	19481	$^4G_{11/2}$	$2\Gamma_6$	21963
	$2\Gamma_6$	12653		$2\Gamma_6$	15915[c]	$^4G_{9/2}$	$\Gamma_{4,5}$	19556		$\Gamma_{4,5}$	21989
$^2H_{9/2}$	$\Gamma_{4,5}$	12669		$\Gamma_{4,5}$	16012[c]		$\Gamma_{4,5}$	19650	$^2K_{15/2}$	$2\Gamma_6$	22209
	$2\Gamma_6$	12869	$^4G_{5/2}$	$\Gamma_{4,5}$	16899	$^2K_{13/2}$	$\Gamma_{4,5}$	19807			
	$\Gamma_{4,5}$	12892	$^4G_{7/2}$	$\Gamma_{4,5}$	16956		$2\Gamma_6$	19990			
$^4F_{7/2}$	$\Gamma_{4,5}$	13363	$^4G_{5/2}$	$2\Gamma_6$	17144						
	$2\Gamma_6$	13508									
					Sm(trensal)						
$^6H_{5/2}$	$\Gamma_{4,5}$	0	$^6F_{1/2}$	$\Gamma_{4,5}$	6618	$^4M_{15/2}$	$2\Gamma_6$	20789	$^4M_{19/2}$	$\Gamma_{4,5}$	23917
	$2\Gamma_6$	277	$^6H_{15/2}$	$2\Gamma_6$	6653	$^4I_{9/2}$	$\Gamma_{4,5}$	20932	$^6P_{5/2}$	$\Gamma_{4,5}$	24003
	$\Gamma_{4,5}$	315	$^6F_{3/2}$	$2\Gamma_6$	6873	$^4I_{11/2}$	$\Gamma_{4,5}$	21020		$\Gamma_{4,5}$	24049
$^6H_{7/2}$	$\Gamma_{4,5}$	1110	$^6H_{15/2}$	$\Gamma_{4,5}$	6967	$^4M_{15/2}$	$\Gamma_{4,5}$	21087	$^4M_{19/2}$	$\Gamma_{4,5}$	24171
	$\Gamma_{4,5}$	1304	$^6F_{5/2}$	$\Gamma_{4,5}$	7372		$\Gamma_{4,5}$	21163	$^6P_{5/2}$	$\Gamma_{4,5}$	24247
	$\Gamma_{4,5}$	1357		$2\Gamma_6$	7457		$2\Gamma_6$	21230	$^4M_{19/2}$	$\Gamma_{4,5}$	24289
	$2\Gamma_6$	1470		$\Gamma_{4,5}$	7520	$^4I_{11/2}$	$2\Gamma_6$	21330		$\Gamma_{4,5}$	24366
$^6H_{9/2}$	$\Gamma_{4,5}$	2332	$^6F_{7/2}$	$2\Gamma_6$	8220		$\Gamma_{4,5}$	21467		$2\Gamma_6$	24449
	$2\Gamma_6$	2429		$\Gamma_{4,5}$	8249	$^4I_{13/2}$	$\Gamma_{4,5}$	21550		$\Gamma_{4,5}$	24533
	$\Gamma_{4,5}$	2504	$^6F_{9/2}$	$\Gamma_{4,5}$	9370	$^4I_{11/2}$	$2\Gamma_6$	21611	$^4L_{13/2}$	$\Gamma_{4,5}$	24593
	$\Gamma_{4,5}$	2617		$\Gamma_{4,5}$	9387	$^4I_{13/2}$	$\Gamma_{4,5}$	21653		$2\Gamma_6$	24703
	$2\Gamma_6$	2669		$2\Gamma_6$	9424		$\Gamma_{4,5}$	21705		$2\Gamma_6$	24813
$^6H_{11/2}$	$2\Gamma_6$	3667		$\Gamma_{4,5}$	9458		$\Gamma_{4,5}$	21780		$\Gamma_{4,5}$	24900
	$\Gamma_{4,5}$	3726		$2\Gamma_6$	9505		$2\Gamma_6$	21838		$\Gamma_{4,5}$	24943
	$\Gamma_{4,5}$	3801	$^4G_{5/2}$	$\Gamma_{4,5}$	17670	$^4F_{5/2}$	$\Gamma_{4,5}$	22113	$^6P_{3/2}$	$\Gamma_{4,5}$	25056
	$2\Gamma_6$	3974		$\Gamma_{4,5}$	18286		$2\Gamma_6$	22162	$^4M_{21/2}$	$\Gamma_{4,5}$	25093
	$\Gamma_{4,5}$	3996	$^4F_{3/2}$	$\Gamma_{4,5}$	18920		$\Gamma_{4,5}$	22415		$2\Gamma_6$	25144
$^6H_{13/2}$	$\Gamma_{4,5}$	5046		$2\Gamma_6$	18938	$^4M_{17/2}$	$2\Gamma_6$	22471	$^4F_{7/2}$	$\Gamma_{4,5}$	25207
	$\Gamma_{4,5}$	5076	$^4G_{7/2}$	$\Gamma_{4,5}$	19891		$\Gamma_{4,5}$	22690	$^4M_{21/2}$	$\Gamma_{4,5}$	25265
	$\Gamma_{4,5}$	5219		$\Gamma_{4,5}$	20026	$^4G_{9/2}$	$2\Gamma_6$	22793		$\Gamma_{4,5}$	25367
	$2\Gamma_6$	5460		$2\Gamma_6$	20213	$^4M_{17/2}$	$\Gamma_{4,5}$	22846	$^4K_{11/2}$	$\Gamma_{4,5}$	25451
	$\Gamma_{4,5}$	5481		$\Gamma_{4,5}$	20250	$^4I_{15/2}$	$2\Gamma_6$	22929			
$^6H_{15/2}$	$\Gamma_{4,5}$	6386	$^4M_{15/2}$	$\Gamma_{4,5}$	20390	$^4G_{9/2}$	$\Gamma_{4,5}$	23185			
	$\Gamma_{4,5}$	6442	$^4I_{9/2}$	$\Gamma_{4,5}$	20549		$\Gamma_{4,5}$	23222			
				$\Gamma_{4,5}$	20715						
					Eu(trensal)						
$^7F_0$	Γ_1	0	$^7F_3$	$\Gamma_{2,3}$	1927	$^7F_5$	$\Gamma_{2,3}$	4042	$^5D_1$	Γ_1	18975
$^7F_1$	Γ_1	210		$\Gamma_{2,3}$	1972		$\Gamma_{2,3}$	4162		$\Gamma_{2,3}$	19021
	$\Gamma_{2,3}$	435		Γ_1	2070		$\Gamma_{2,3}$	4350	$^5D_2$	$\Gamma_{2,3}$	21394
$^7F_2$	$\Gamma_{2,3}$	817		Γ_1	2152	$^7F_6$	$\Gamma_{2,3}$	4935		Γ_1	21455
	Γ_1	870	$^7F_4$	Γ_1	2505		Γ_1	4980		$\Gamma_{2,3}$	21529
	$\Gamma_{2,3}$	1327		$\Gamma_{2,3}$	3127	$^5D_0$	Γ_1	17257			
				Γ_1	3202						
				$\Gamma_{2,3}$	3247						
					Tb(trensal)						
$^7F_6$	Γ_1	0	$^7F_2$	$\Gamma_{2,3}$	5140	$^7F_1$	$\Gamma_{2,3}$	5806	$^5D_4$	Γ_1	20537
$^7F_3$	Γ_1	4570		Γ_1	5561	$^7F_0$	Γ_1	6096		$\Gamma_{2,3}$	20548
	$\Gamma_{2,3}$	4589		$\Gamma_{2,3}$	5591					$\Gamma_{2,3}$	20569
	$\Gamma_{2,3}$	4633								Γ_1	20587
	Γ_1	4674								$\Gamma_{2,3}$	20609
										Γ_1	20627
					Dy(trensal)						
$^6H_{15/2}$	$\Gamma_{4,5}$	0	$^6H_{9/2}$	$2\Gamma_6$	8030	$^6F_{7/2}$	$\Gamma_{4,5}$	11135	$^4I_{15/2}$	$\Gamma_{4,5}$	21860
$^6H_{11/2}$	$\Gamma_{4,5}$	5936		$\Gamma_{4,5}$	8079		$\Gamma_{4,5}$	11280		$2\Gamma_6$	21953
	$2\Gamma_6$	5954	$^6F_{11/2}$	$2\Gamma_6$	8258		$2\Gamma_6$	11307		$\Gamma_{4,5}$	22082[c]
	$\Gamma_{4,5}$	5977		$\Gamma_{4,5}$	8355		$\Gamma_{4,5}$	11361		$2\Gamma_6$	22328
	$\Gamma_{4,5}$	6099	$^6F_{9/2}$	$2\Gamma_6$	8957	$^6F_{5/2}$	$\Gamma_{4,5}$	12528		$\Gamma_{4,5}$	22376
	$2\Gamma_6$	6189	$^6H_{7/2}$	$\Gamma_{4,5}$	9053		$2\Gamma_6$	12598		$2\Gamma_6$	22417
$^6H_{9/2}$	$2\Gamma_6$	7661	$^6F_{9/2}$	$2\Gamma_6$	9301		$\Gamma_{4,5}$	12707		$\Gamma_{4,5}$	22474
	$\Gamma_{4,5}$	7729		$\Gamma_{4,5}$	9363	$^6F_{3/2}$	$\Gamma_{4,5}$	13392	$^4G_{11/2}$	$\Gamma_{4,5}$	23400
$^6F_{11/2}$	$\Gamma_{4,5}$	7802	$^6H_{7/2}$	$\Gamma_{4,5}$	9424		$2\Gamma_6$	13418		$2\Gamma_6$	23437
	$2\Gamma_6$	7830	$^6F_{9/2}$	$2\Gamma_6$	9468	$^4F_{9/2}$	$2\Gamma_6$	20897		$\Gamma_{4,5}$	23715
	$\Gamma_{4,5}$	7986	$^6H_{7/2}$	$\Gamma_{4,5}$	9686		$\Gamma_{4,5}$	20908			
							$\Gamma_{4,5}$	21023			
							$2\Gamma_6$	21164			

Table 2. Continued

multiplet[b]		energy obsd	multiplet[b]		energy obsd	multiplet[b]		energy obsd	multiplet[b]		energy obsd
					Ho(trensal)						
$^5I_8$	Γ_1	0	$^5F_5$	$\Gamma_{2,3}$	15445	$^5F_3$	Γ_1	20536	$^5G_6$	Γ_1	21958
$^5I_7$	Γ_1	5235		Γ_1	15467		$\Gamma_{2,3}$	20657		Γ_1	21982
	$\Gamma_{2,3}$	5256		$\Gamma_{2,3}$	15494		Γ_1	20682		$\Gamma_{2,3}$	22004
	$\Gamma_{2,3}$	5263		Γ_1	15600		Γ_1	20738		$\Gamma_{2,3}$	22050
	Γ_1	5446		$\Gamma_{2,3}$	15701		$\Gamma_{2,3}$	20799		Γ_1	22280
$^5I_6$	$\Gamma_{2,3}$	8740		Γ_1	15754	$^5F_2$	$\Gamma_{2,3}$	21101		$\Gamma_{2,3}$	22401
	Γ_1	8750		$\Gamma_{2,3}$	15765		Γ_1	21151	$^5F_1$	Γ_1	22475
	$\Gamma_{2,3}$	8759	$^5S_2$	$\Gamma_{2,3}$	18449		$\Gamma_{2,3}$	21234		$\Gamma_{2,3}$	22503
	Γ_1	8784		$\Gamma_{2,3}$	18534	$^3K_8$	Γ_1	21299	$^5G_5$	Γ_1	23888
	Γ_1	8840	$^5F_4$	$\Gamma_{2,3}$	18584		$\Gamma_{2,3}$	21328		$\Gamma_{2,3}$	23904
	$\Gamma_{2,3}$	8885		$\Gamma_{2,3}$	18633		Γ_1	21342		$\Gamma_{2,3}$	24036
	Γ_1	8976		Γ_1	18644		$\Gamma_{2,3}$	21375		Γ_1	24120
	Γ_1	8985		$\Gamma_{2,3}$	18716		Γ_1	21400		$\Gamma_{2,3}$	24146
				Γ_1	18722		$\Gamma_{2,3}$	21498		Γ_1	24168
							Γ_1	21529	$^5G_6$	Γ_1	21958
							$\Gamma_{2,3}$	21570			
							$\Gamma_{2,3}$	21595			
							Γ_1	21604			
					Tm(trensal)						
$^3H_6$	Γ_1	0	$^3H_5$	$\Gamma_{2,3}$	8323	$^3H_4$	$\Gamma_{2,3}$	12630	$^3F_2$	$\Gamma_{2,3}$	15269
	Γ_1	20		$\Gamma_{2,3}$	8556		$\Gamma_{2,3}$	12862		Γ_1	15339
$^3F_4$	Γ_1	5594		Γ_1	8586		Γ_1	12873		$\Gamma_{2,3}$	15553
	$\Gamma_{2,3}$	5814		Γ_1	8622		Γ_1	13054	$^1G_4$	$\Gamma_{2,3}$	21179
	Γ_1	6080		$\Gamma_{2,3}$	8799		$\Gamma_{2,3}$	13138		$\Gamma_{2,3}$	21721
	$\Gamma_{2,3}$	6188				$^3F_3$	Γ_1	14664		$\Gamma_{2,3}$	21862
	Γ_1	6239					$\Gamma_{2,3}$	14751			
							Γ_1	14856			

[a] Data for Er(trensal) are given in ref 8. [b] The principal multiplet component in the wave function. [c] Levels that were not included in the fit (see the text).

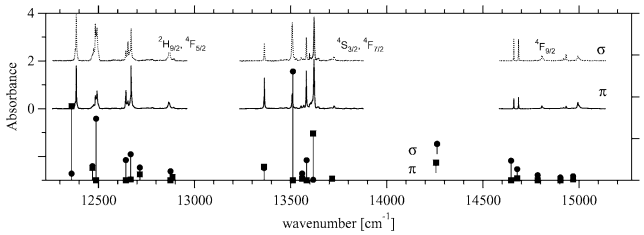

Figure 4. Near-IR spectra of Nd(trensal) at 10 K. Stick spectra are the calculated energies and relative intensities.

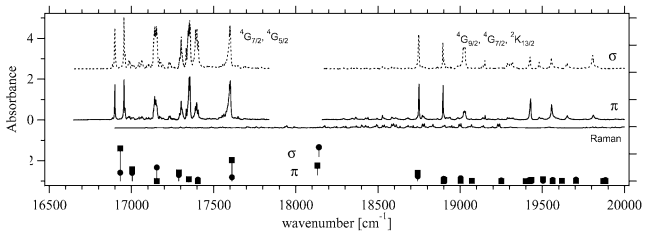

Figure 5. A portion of the visible spectrum of Nd(trensal) at 10 K. Stick spectra are the calculated energies and relative intensities. The Raman spectra convoluted with the intense $^4G_{7/2}$ and $^4G_{5/2}$ multiplet origins are shown to occur in the region of the weak lines centered at ~18500 cm^{-1}.

intensities are not observed due to the absorption saturation (Figure 5, σ polarization).

Figure 5 also illustrates the vibronic activity of the ligand vibrations in particular transitions. The weak peaks on the low-energy side of the $^4G_{9/2}$ multiplet around 18500 cm^{-1} appear to be vibronic transitions based on the intense $^4G_{7/2}$,$^4G_{5/2}$ origins. The Raman spectrum of Nd(trensal) convoluted with the $^4G_{7/2}$,$^4G_{5/2}$ origins is shown for illustration. It appears that some ring stretching vibrations are coupled to the f−f electronic lanthanide transitions. As observed previously for Er(trensal), this vibronic activity can be relatively intense if it coincides with the electronic transitions of a higher energy multiplet.

Table 3. Electric Dipole Selection Rules in C_3 Symmetry

even electrons	σ	π	odd electrons	σ	π
$\Gamma_1 \rightarrow \Gamma_1$	F[b]	A[b]	$\Gamma_{4,5} \rightarrow \Gamma_{4,5}$	A	A
$\rightarrow \Gamma_{2,3}$[a]	A	F	$\rightarrow \Gamma_6$	A	F
$\Gamma_{2,3} \rightarrow \Gamma_1$	A	F	$\Gamma_6 \rightarrow \Gamma_{4,5}$	A	F
$\rightarrow \Gamma_{2,3}$	A	A	$\rightarrow \Gamma_6$	F	A

[a] $\Gamma_{2,3}$ denotes the (Γ_2, Γ_3) degenerate pair, while $\Gamma_{4,5}$ and Γ_6 are the Kramers doublets (Γ_4, Γ_5) and (Γ_6, Γ_6), respectively. [b] A = allowed; F = forbidden.

Ligand-Field Calculations. A conventional electronic Hamiltonian is used that has both atomic and ligand-field parameters. The main atomic parameters include an average energy or offset term, E_{av}, the electron repulsion parameters, F^k (k = 2, 4, 6), and the spin−orbit coupling constant, ζ_{so}. It was found that the "minor" atomic parameters α, β, γ, T^i (i = 2, 3, 4, 6, 7, 8), P^k (k = 2, 4, 6), and M^j (j = 0, 2, 4) have little influence on the fit over the range of levels being studied. A number of different sets resulted in near identical fits or in some of the parameters wandering from generally accepted values. Finally, these 15 minor parameters were all fixed at the free-ion values. These values can be found in Table 5 of ref 16. This table is also reproduced in the Supporting Information. The ligand field was expanded in terms of the one-electron spherical tensor operators C_{kq},

(16) Goerller-Walrand, C.; Binnemans, K. In *Handbook on the Physics and Chemistry of Rare Earths*; Gschneidner, K. A., Eyring, L., Eds.; North-Holland: Amsterdam, 1996; Vol. 23, p 121.

Table 4. Parameters of the Ligand-Field Hamiltonian[a] for the Ln(trensal) Complexes

	Pr	Nd	Sm	Eu	Tb	Dy	Ho	Er	Tm
E_{av}	10342	24190	47685	62952	68097	55806	48195	35662	18147
F^2	67382	71251	79214	80729	89540[e]	92822	94952	98935	100700
F^4	49747	51889	56422	58315	63485[e]	66962	68620	70940	70985
F^6	33101	35145	40238	42894	43345	46798	46835	49585	50291
ξ_{SO}	737	870	1174	1333	1705[e]	1878	2118	2371	2626
B_{20}	−901(102)	−848(78)	−770(48)	−868(29)	−617(211)	−671(39)	−316(103)	−720(59)	−952(62)
B_{40}	139(176)	−109(135)	−46(85)	−45(63)	89(255)	−186(77)	−186(136)	−44(106)	86(87)
B_{43}[c]	−2673(67)	−2404(66)	−2307(47)	−2269(36)	−1928(161)	−2153(34)	−1910(58)	−2121(83)	−1780(42)
B_{60}	1702(139)	1725(143)	1563(85)	1699(56)	1582(985)	1241(57)	1146(132)	988(36)	1168(70)
B_{63}	605 + i40	556 − i254	400 + i463	751 + i256	719 + i129	439 − i284	732 − i281	353 + i92	143 − i270
	(140, i−)	(129, i 490)	(72, i135)	(44, i276)	(717, i−)	(41, i83)	(100, i170)	(49, i53)	(72, i222)
B_{66}	653 + i92	1081 + i119	386 + i374	343 − i101	1103 + i266	660 + i145	460 + i570	545 + i311	801 − i119
	(107, i−)	(145, i 753)	(108, i142)	(82, i426)	(420, i−)	(49, i137)	(119, i133)	(34, i36)	(75, i228)
$N_v/(4\pi)^{1/2}$	1449	1401	1261	1278	1173	1163	1054	1122	1052
N[b]	23	54	94	25	16	44	59	52	26
σ[d]	19	23	24	7	24	12	15	20	11

[a] All parameters except N in cm^{-1}. The "minor" atomic parameters are taken from ref 16. The numbers in parentheses are the uncertainties. [b] Number of assigned energy levels included in the fit. [c] The *x* and *y* axes can always be chosen to make B_{43} real; see the text. [d] Root-mean-squared deviation between calculated and observed energies. [e] Parameter not varied.

which in C_3 symmetry can be expressed as[16]

$$H_{CF} = B_{20}C_{20} + B_{40}C_{40} + \mathrm{Re}(B_{43})(C_{4-3} - C_{43}) + \mathrm{i}[\mathrm{Im}(B_{43})](C_{4-3} + C_{43}) + B_{60}C_{60} + \mathrm{Re}(B_{63})(C_{6-3} - C_{63}) + \mathrm{i}[\mathrm{Im}(B_{63})](C_{6-3} + C_{63}) + \mathrm{Re}(B_{66})(C_{6-6} + C_{66}) + \mathrm{i}[\mathrm{Im}(B_{66})](C_{6-6} - C_{66}) \quad (1)$$

where Re(*x*) and Im(*x*) denote the real and imaginary parts of the complex number *x*. It is well known that the values of the B_{kq} coefficients of a ligand field are dependent on the coordinate system used (see pp 150−152, ref 16). In particular, the same ligand field can be generated using different B_{kq} values, which can cause great confusion when values in the literature are compared. For this reason, conventions are used to define the axes.[16,17] These conventions are that the *z* axis is coincident with the principal axis, the *y* axis is coincident with an orthogonal C_2 axis (if it exists), and the *x* axis completes a right−handed coordinate system.

While it is always possible to define a ligand field of a particular symmetry in terms of a greater number of B_{kq} parameters (corresponding to an inappropriate choice of coordinate system), there are symmetry-determined *minimal* sets of B_{kq} parameters for particular point groups. These sets of *independent* nonvanishing B_{kq} parameters are given, for example, in Table 5 of ref 17. In this table, for a ligand field of C_3 symmetry the Im(B_{43}) parameter is zero. Thus, the *minimal* number of B_{kq} parameters to *fully* describe a C_3 ligand field is eight not nine as given in eq 1.

The nine parameters given in eq 1 are not the symmetry-determined minimal set of B_{kq} parameters. This is because the directions of the *x* and *y* axes are not defined in the C_3 point group. If we calculate the C_3 ligand field using a general orientation of the *x* and *y* axes, then a nonzero Im(B_{43}) is calculated. However, as discussed further below, there is a particular orientation (not defined by symmetry) where Im(B_{43}) is zero. We calculate the B_{kq} parameters as the *x* and *y* axes are rotated about the *z* axis, until an orientation is found where the Im(B_{43}) vanishes. We have then calculated the minimal set of eight parameters to describe the C_3 point group. The experimental energy levels are fitted to the minimal set of eight crystal-field parameters, B_{20}, B_{40}, Re(B_{43}), B_{60}, Re(B_{63}), Im(B_{63}), Re(B_{66}), and Im(B_{66}) (those of eq 1 with Im(B_{43}) set to zero), using the previously found values for Er(trensal) as a starting point.[8] The experimental and calculated values were refined to give the crystal-field parameters in Table 4. Many different starting sets were also tried. Occasionally a fit would converge into a local minimum, and an adjustment of the starting parameters was required. In the case of Tb(trensal) there was insufficient experimental data to determine all parameters, and in this case F^2, F^4, and ζ_{so} were fixed to their free-ion values. The uncertainties of the fitted parameters are given in parentheses in Table 4. In some cases the uncertainties in Im(B_{63}) and Im(B_{66}) were too large to be estimated accurately. The crystal-field parameters are shown in Figure 6 together with their uncertainties; the uncertainties in Im(B_{63}) and Im(B_{66}) for the Pr and Tb complexes have been set to ±1000 cm^{-1}.

Table 5. AOM Structural and Bonding Parameters for Ln(trensal)

ligand		AOM angles[a]			AOM parameters		
	i	θ_i	ϕ_i	ψ_i	$e_\sigma(i)$	$e_{\pi x}(i)$	$e_{\pi y}(i)$
N1	1	0	ϕ[b]	0	σ(N1)	0	0
N2	2	θ_{N2}	ϕ	ψ_{N1}	σ(N2)	0	π_y(N2)
N2′	3	θ_{N2}	$\phi + 120°$	ψ_{N1}	σ(N2)	0	π_y(N2)
N2″	4	θ_{N2}	$\phi + 240°$	ψ_{N1}	σ(N2)	0	π_y(N2)
O	5	θ_O	$\phi + \phi_O$	ψ_O	σ(O)	0	π_y(O)
O′	6	θ_O	$\phi + \phi_O + 120°$	ψ_O	σ(O)	0	π_y(O)
O″	7	θ_O	$\phi + \phi_O + 240°$	ψ_O	σ(O)	0	π_y(O)

[a] θ_{N2}, θ_O, ϕ_O, ψ_{N2}, and ψ_O are given in Table 1. [b] ϕ determines the orientation of the *x* and *y* axes; see the text.

There are some anomalous multiplets whose calculated positions are known to deviate from their experimentally observed values due to their dependence on the two-electron operators of the correlated crystal-field model.[16] Since this would distort our fit to a simple one-electron operator model, we do not include these levels in the fit. The levels omitted are the $^1D_2$(Pr) and the $^2H(2)_{11/2}$(Nd) multiplets and are

(17) Morrison, C. A.; Leavitt, R. P. In *Handbook on the Physics and Chemistry of the Rare Earths*; Gschneidner, K. A., Eyring, L., Eds.; North-Holland: Amsterdam, 1982; Vol. 5, p 461.

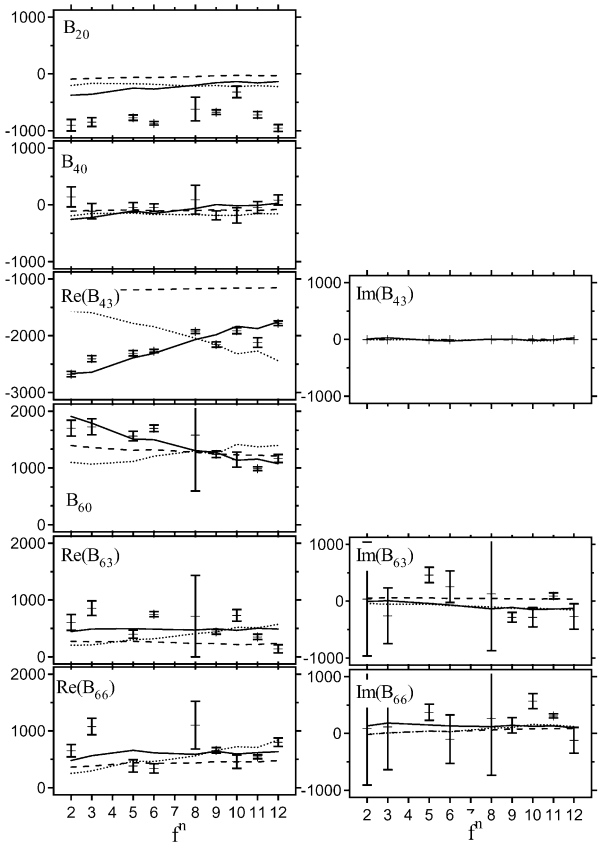

Figure 6. Variation of the B_{kq} crystal-field parameters across the Ln(trensal) series. The experimental data are shown with their standard deviations as error bars: dashed line, AOM parameters fixed at $\sigma(N1) = \sigma(N2) = \sigma(O) = 300$ cm^{-1} and $\pi_\perp(N2) = \pi_\perp(O) = 100$ cm^{-1}; dotted line, a global fit assuming $\sigma \propto R^{-8}$ dependence, $e_\sigma(N1) = 345$ cm^{-1}, $e_\sigma(N2) = 670$ cm^{-1}, $e_\sigma(O) = 325$ cm^{-1}, $\pi_\perp(N2) = 243$ cm^{-1}, and $\pi_\perp(O1) = 349$ cm^{-1}; solid line, a global fit assuming $\sigma \propto R^{8}$ dependence, $e_\sigma(N1) = 384$ cm^{-1}, $e_\sigma(N2) = 742$ cm^{-1}, $e_\sigma(O) = 258$ cm^{-1}, $\pi_\perp(N2) = 244$ cm^{-1}, and $\pi_\perp(O1) = 379$ cm^{-1}. A value of $\phi = -4.2°$ was used to define the X and Y axes.

marked with asterisks in Table 2. The necessity of including the correlated crystal-field model operators in accounting for the energy levels of these particular transitions has been previously discussed for Pr[18] and Nd[19] complexes.

Discussion

Ligand-Field Strength. The ligand field that the lanthanide ions experience from the trensal ligand is large and can be quantified by the parameter $N_v/(4\pi)^{1/2}$:

$$N_v/(4\pi)^{1/2} = \left[\sum_{k=2,4,6} \frac{1}{2k+1}(B_{k0}{}^2 + 2\sum_{q=1}^{k}|B_{kq}|^2)\right]^{1/2} \quad (2)$$

A plot of $N_v/(4\pi)^{1/2}$ together with the bond lengths for Ln(trensal) as a function of the lanthanide ion is given in Figure 7. This clearly shows that both the large values for the ligand field and the general trend for the ligand-field strength *decrease* with increasing atomic number along the series. This decrease of bonding strength, together with the contraction in the bond length along the series, may at first seem counterintuitive. However, it indicates that the contraction of the f orbitals along the series decreases the metal−ligand orbital overlap to a greater extent than the decrease of the bond lengths increases the metal−ligand orbital overlap.[20] Similar trends have previously been observed[21,22] and will be discussed further in the following sections.

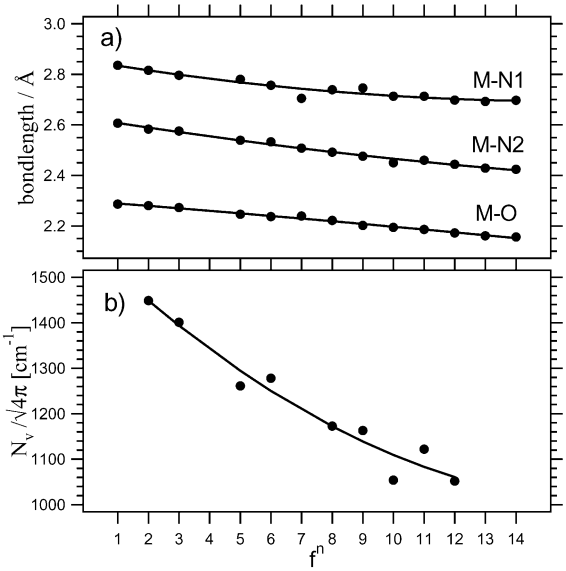

Figure 7. Variation of (a) the bond lengths and (b) the ligand-field strength in Ln(trensal) complexes as a function of the lanthanide ion. The lines are guides for the eye.

Structural Variations. The contraction of the metal−ligand bond lengths on going from left to right across the lanthanide series shown in Figure 7 also results in a systematic change in their angular disposition. We use the usual three AOM angles θ, ϕ, and ψ to describe the orientation of the coordinating atoms.[23] These angles define the transformation from an x_M, y_M, z_M metal-based axis system to each x_L, y_L, z_L axis system based on the coordinating atoms. Figure 8 shows the variation in these angles as a function of the lanthanide. The first two angles, θ and ϕ, determine the position of the coordinating atom, while the third, ψ, specifies the orientation of the x_L, y_L axes perpendicular to the bond. The angle ψ can be used to describe anisotropy in the π-bonding; for isotropic π-bonding ψ can be set to zero. Using Figure 1, we define a molecular coordinate system where the Z axis is coincident with the C_3 axis, the Y axis is perpendicular to the plane defined by the Ln, N1, and N2 atoms, and the X axis completes a right-handed coordinate system. We then take the x_M, y_M, z_M metal-centered axes initially coincident with the fixed X, Y, Z molecular axes. For each ligand, θ_i gives the rotation of the x_M, y_M, z_M axes about the Y axis; ϕ_i is the rotation about the Z axis away from the XZ plane. The x_M, y_M, z_M axes are now centered on the coordinating atom, and the angle ψ_i is the rotation of these axes about the bond to make the x_M, y_M, z_M axes coincident with the x_L, y_L, z_L axes.

(18) Judd, B. R. *J. Lumin.* **1979**, *18/19*, 604.
(19) Faucher, M.; Garcia, D.; Caro, P.; Derouet, J.; Porcher, P. *J. Phys. (Paris)* **1989**, *50*, 219.
(20) Axe, J. D.; Burns, G. *Phys. Rev.* **1966**, *152*, 331.
(21) Linares, C.; Louat, A.; Blanchard, M. *Chem. Phys.* **1982**, *68*, 453.
(22) Urland, W. *Chem. Phys. Lett.* **1977**, *50*, 445.
(23) Schäffer, C. E. *Struct. Bonding (Berlin)* **1968**, *5*, 68.

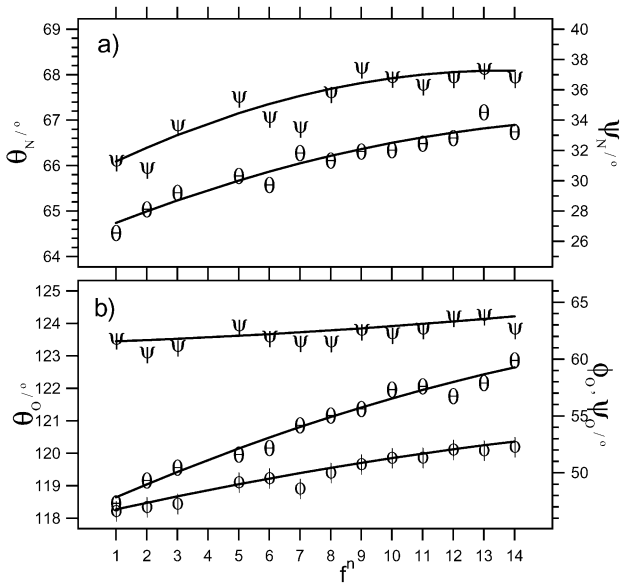

Figure 8. Variation of the AOM angles θ, ϕ, and ψ for (a) N2 and (b) O coordinating atoms in Ln(trensal).

For the present series of complexes with C_3 symmetry, the *position* of the seven coordinating atoms can then be defined by the three independent bond lengths (Ln−N1, Ln−N2, Ln−O) and the angles θ_{N2}, θ_O, and ϕ_O. However, a π-bonding anisotropy of the N2 and O coordination is expected with respect to the aromatic planes of the three six-membered bidentate rings. Two further angles, ψ_{N2} and ψ_O, describe the orientation of these planes. The angles ψ_{N2} and ψ_O are determined by the angle between the Ln−N2−C3 and N1−Ln−N2 planes and the Ln−O−C5 and N1−Ln−O planes, respectively.

Apart from these structural parameters, the AOM description of the ligand field requires three e_σ parameters to describe the σ-bonding and four e_π parameters, $e_{\pi x}$(N2), $e_{\pi y}$(N2), $e_{\pi x}$(O), and $e_{\pi y}$(O), to describe the π-bonding. We assume that $e_\pi = 0$ for the saturated amine (N1). The angles and AOM parameters that describe this for the general Ln(trensal) complex are given in Table 5. The actual angles together with the three independent bond lengths are those given in Table 1.

Figures 7 and 8 illustrate the systematic manner in which the geometry of the Ln(trensal) complexes changes across the lanthanide series. The bond lengths follow the expected lanthanide contraction. The apical nitrogen forms the longest bond, and this atom is nonbonded in transition-metal complexes.[24] The large difference in the bond length of the imine N2 and phenolate O1 reflects the preference of lanthanide ions for oxygen ligands. The contraction of the bond lengths across the series also results in the observed systematic angular changes: an increase in θ_{N2}, θ_O, and ϕ_O. This indicates that the heptadentate trensal ligand can extend its grip further *down* (the θ_{N2} and θ_O angles increase) and *around* (the ϕ_O angle increases) the metal ion as the coordinate bonds contract. The trend with the ψ_{N2} and ψ_O angles is also for a general increase along the series, although here there is a larger scatter of values.

Rationalizing the Ligand Field in Terms of the AOM Model. The relationship between the B_{kq} crystal-field parameters and the AOM parameters has been discussed previously and the AOM rotational matrix, which allows anisotropic π-bonding to be incorporated into the calculation, has been given.[8] In principle the crystal-field parameters, B_{kq}, can be expressed as a function of the angular coordinates θ_j, ϕ_j, and ψ_j of the ligands and the bonding parameters $e_t(j)$ ($t = \sigma, \pi_x, \pi_y$) using the methods of Urland.[25] In what follows we have used the explicit fixed geometry for each Ln(trensal) complex from the structural data (Table 1) and expressed the B_{kq} parameters in terms of the AOM parameters. We then determine the AOM parameters that most closely reproduce the B_{kq} values that were obtained from fitting the experimental energy levels.

We wish to see how far the B_{kq} parameters can be rationalized in terms of local metal−ligand bonding. A preliminary study on the Er(trensal) complex[8] indicated that unusually large π parameters were required, although it was not clear whether this was a general trend property of the trensal ligand, or a failure of the ligand field being expressed in terms of the local bonding. The AOM approach was also used to check the consistency of the fitted B_{kq} values with regard to sign ambiguities. It is of interest in this study whether the AOM may be used to rationalize variations in the ligand-field parameters along the Ln(trensal) series in terms of the structural trends. It is important to stress that the AOM uses the *actual* molecular geometry rather than the molecular symmetry of the problem.

In all complexes the $e_{\pi\|}$(N2) and $e_{\pi\|}$(O) parameters for π-bonding within the plane of the bidentate ring were found to be close to zero. Therefore, in the present case we require only five AOM parameters to describe the problem (three σ-bonding parameters for the three independent bonding atoms and two π-bonding parameters for the N2 and O atoms), whereas the crystal-field approach requires the eight parameters B_{20}, B_{40}, Re(B_{43}), B_{60}, Re(B_{63}), Im(B_{63}), Re(B_{66}), and Im(B_{66}).

As discussed previously,[8] the AOM description of the ligand field has an inherent advantage in being able to treat a low-symmetry molecule with a known geometry using a smaller number of parameters. However, an additional complication is introduced if the axes are not symmetry determined. In Ln(trensal) complexes the position of the X and Y axes are arbitrary within the plane perpendicular to the 3-fold axis. The choice of how the X and Y axes are defined changes the phase of the $B_{kq}(q \neq 0)$ values,[26] and a general choice will introduce a nonzero Im(B_{43}). We define an additional angle, ϕ, that the X axis makes with the N2−Ln−N1 plane. There exists a value of ϕ (and $\phi + 120°$, $\phi + 240°$) in which Im(B_{43}) = 0. In the C_3 point group the value of ϕ is not symmetry determined and is a complicated function of both the geometry *and* the bonding parameters.

(24) Chandra, S. K.; Chakravorty, A. *Inorg. Chem.* **1991**, *30*, 3795.

(25) Urland, W. *Chem. Phys.* **1976**, *14*, 393.

(26) Rudowicz, C. *J. Chem. Phys.* **1986**, *84*, 5045.

Table 6. Equivalent Ligand Fields for C_3 Symmetry[a]

ϕ/deg	Re(B_{43})	Im(B_{43})	Re(B_{63})	Im(B_{63})	Re(B_{66})	Im(B_{66})
30	Im(B_{43})	−Re(B_{43})	Im(B_{63})	−Re(B_{63})	−Re(B_{66})	−Im(B_{66})
60	−Re(B_{43})	−Im(B_{43})	−Re(B_{63})	−Im(B_{63})	Re(B_{66})	Im(B_{66})
90	−Im(B_{43})	Re(B_{43})	−Im(B_{63})	Re(B_{63})	−Re(B_{66})	−Im(B_{66})
120	Re(B_{43})	Im(B_{43})	Re(B_{63})	Im(B_{63})	Re(B_{66})	Im(B_{66})

[a] The B_{20}, B_{40}, and B_{60} parameters do not change as a function of ϕ.

It is important to specify this angle ϕ; otherwise, the crystal-field and AOM calculations are effectively using different coordinate systems and the parameters cannot be directly compared. Not only will Im(B_{43}) be nonzero, but also the phase of *all* $B_{kq}(q \neq 0)$ parameters will change. The values $\phi = 120°$, 240°, and 360° in Table 5 result in the same ligand field (and energy levels) and the same ligand-field parameters. The values $\phi = 30°$, 60°, 90°, ... also result in the same ligand field, but are expressed by different ligand-field parameters as shown in Table 6. Note that with the usual definition of a C_3 ligand field with Im(B_{43}) = 0, changing the sign of both Re(B_{43}) and B_{63} by setting $\phi = 60°$ results in the *same* ligand field as $\phi = 0°$.

In the fitting procedure, we numerically calculate the value of ϕ that satisfies the condition Im(B_{43}) = 0. In this way we can directly compare the B_{kq} values from different calculations. The required expressions for the B_{kq} parameters in terms of the AOM parameters were derived using Mathematica. The resulting long and complicated expressions are derived for the particular geometry for each of the Ln(trensal) complexes in Table 1. These expressions are not repeated here (see the Supporting Information) but can be used to calculate B_{kq} numerically by fitting the $e_t(j)$ AOM parameters to the B_{kq} values found from experiment.

The lines given in Figure 6 show the B_{kq} values calculated for particular sets of AOM parameters. The dashed line is for all coordinating atoms set to $e_\sigma = 300$ cm^{-1} and $e_{\pi\perp} = 100$ cm^{-1} for N2 and O, typical values found from fitting other lanthanide complexes to AOM parameters.[21,22] While the same values are used for all lanthanides, ϕ is adjusted in each case to give Im(B_{43}) = 0. Note that even at this level of approximation the signs of the B_{kq} parameters are correctly predicted. It is noted that the AOM parameters are quite sensitive to particular B_{kq} values. For example, if B_{40} is small, it forces σ(N1) to also be small, because B_{40} depends mainly on the $\langle z^3|V|z^3\rangle$ matrix element.[25] Only a small variation of these calculated parameters is seen (dashed line in Figure 6) as a function of the lanthanide, although significant variation is observed experimentally for Re(B_{43}) and B_{60}. A large discrepancy between the calculated and experimental values of B_{20} and Re(B_{43}) is seen. The calculation of B_{20} is known to be difficult as it depends on long-range interactions and has a large electrostatic component,[22,27] so we leave out B_{20} in the fitting to the AOM parameters. It was found in attempts to fit to the B_{20} values that (meaningless) negative e_σ parameters resulted. From this and other calculations, it appears that the variation of the B_{kq} parameters as a function of lanthanide cannot be accounted for by the systematic angular changes in the Ln(trensal) geometry alone.

Table 7. AOM Parameters Fitted to the Crystal-Field Parameters for Ln(trensal) Complexes

σ(N1)/cm^{-1}	384	$\pi_\perp$(N2)/cm^{-1}	244
σ(N2)/cm^{-1}	742	$\pi_\perp$(O)/cm^{-1}	379
σ(O)/cm^{-1}	258	ϕ/deg	∼−4.2

The radial variation in geometry of the Ln(trensal) complexes shown by the change in bond lengths in Figure 8 suggests a systematic change in the AOM parameters. For a particular lanthanide with identical ligands at various bond lengths, the AOM σ-bonding parameters are related by $e_{\sigma1}/e_{\sigma2} = (R_2/R_1)^8$.[20,21] This reflects the dependence of the square of the diatomic overlap of the p_σ and f orbitals on bond length close to the equilibrium value. Using such a dependence for the AOM parameters of different lanthanides and allowing the e_σ and e_π parameters to differ for the three independent coordinating atoms result in the B_{kq} values given by the dotted lines in Figure 6. Here the bond lengths of Tb(trensal) are used as a reference geometry and the AOM parameters determined for this complex. The AOM parameters for the other complexes are then given by $e_\sigma^{Ln} = e_\sigma^{Tb}[R(Tb-N2)/R(Ln-N2)]^8$.

In this case the calculated variation of Re(B_{43}) and B_{60} with the lanthanide ion is the *opposite* of what is observed experimentally. As mentioned previously, this indicates that while the bond lengths decrease along the series, one does not find the expected increase in the e_σ parameters as the diatomic overlap decreases due to the contraction of the f orbitals. The f orbital contraction has a greater effect than the bond length decrease. This decreasing overlap with decreasing bond length has also been seen in calculations on the Ln−F series.[20]

While the decrease in the bond length is related to the f orbital contraction, it is not clear how to quantify this. However, if it is assumed that a particular bond length decrease goes with a proportionally larger f orbital contraction, then the relationship for AOM parameters of different lanthanides is the inverse of the expression given above. If we use this relationship with respect to the reference Tb(trensal) geometry, $e_\sigma(j)^{Ln} = e_\sigma(j)^{Tb}[R(Tb-j)/R(Ln-j)]^{-8}$, for j = N1, N2, and O and similar expressions for $e_{\pi\perp}$, the resulting B_{kq} parameters are shown as the solid lines of Figure 6. Apart from the B_{20} value, which was not fitted, good agreement is found for both the magnitude and the trend of the B_{kq} parameters. The resulting AOM parameters are given in Table 7. The value of ϕ required to make Im(B_{43}) = 0 was similar in all cases, $\phi \approx -4.2$. In addition it was found that $e_{\pi|} \approx 0$ for both N2 and O atoms.

As found previously for Er(trensal),[8] the e_σ AOM parameters are an order of magnitude smaller than typically found for transition-metal complexes,[28−30] which is not surprising

(27) Huefner, S. *Optical Spectra of Transparent Rare Earth Compounds*; Academic Press: New York, 1978.

(28) Gerloch, M.; Slade, R. C. *Ligand-Field Parameters*; Cambridge University Press: Cambridge, U.K., 1973.

(29) Lever, A. B. P. *Inorganic Electronic Spectroscopy*, 2nd ed.; Elsevier: Amsterdam, 1984.

(30) Figgis, B. N.; Hitchman, M. A. *Ligand Field Theory and its Applications*; Wiley-VCH: New York, 2000.

Scheme 1

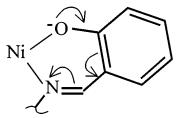

due to the shielded nature of the f electrons. The observation that $\sigma(N1) < \sigma(N2)$ make sense as the bond to the amine (N1) is far longer than to the imine (N2). The $\sigma(N2)/\pi(N2)$ ratio of ~3 is reasonable, but the $\sigma(O)/\pi(O)$ ratio of <1 requires some comment.

There is the question of whether the relatively large AOM π-bonding parameters represent actual π-bonding or whether they are artifacts of the fitting process. Previous studies on the role of π-bonding in lanthanide complexes have seen trends similar to that observed here.[21,31] In a study of Cs_2NaMCl_6 epasolites, a consistent fit of AOM parameters was obtained for a series of six lanthanides. The e_σ/e_π ratio was found to be ~2.5, about half the ratio typically found for transition-metal chlorides.[29] The relatively larger π-bonding found in the present study may be due to the aromatic nature of the phenolate ligand.

Comparison with Transition-Metal Complexes. The bis(*N*-isopropylsalicylideneiminato)nickel complex has been the subject of optical and magnetic studies,[32−34] and the following AOM parameters have been assigned: $\sigma(N) = 4000$ cm^{-1}, $\pi_\perp(N) = 900$ cm^{-1}, $\sigma(O) = 4000$ cm^{-1}, $\pi_\perp(O) = 800$ cm^{-1}, $\pi_{||}(O) = 600$ cm^{-1}. Here it was found[34] that a Schiff-base-type imine acts as a moderate π donor as compared to diimine ligators that act as weak π acceptors, $\pi_\perp = -250$ cm^{-1}. It has been argued that the nearby electron-rich phenolic oxygen atom causes the π electron drift as shown in Scheme 1. The $\pi_{||}(N) = 0$ is justified by the sp^2 description of the N imine and π delocalization. For the phenolic oxygen in the bis(*N*-isopropylsalicylideneiminato)nickel complex the nonzero value for π donation *in* the plane of the aromatic ring ($\pi_{||}$) was rationalized in terms of "misdirected" valency, which causes $\sigma-\pi$ cross terms in the local M−O framework.[34]

The present results for the Ln(trensal) complexes shown in Table 7 concur with these ideas to some extent. Positive $\pi_\perp(N2)$ and $\pi_\perp(O)$ values were found as well as $\pi_{||}(N2) = 0$. Unlike the bis(*N*-isopropylsalicylideneiminato)nickel complex discussed above, markedly worse agreement was found when $\pi_{||}(O)$ was allowed to be nonzero. Therefore, we do not need to invoke misdirected valency to explain a nonzero $\pi_{||}(O)$. The small value of $\sigma(O)$ cannot be explained in terms of misdirected valency either. The net effect of misdirected valency is the scrambling of σ and π parameters so that it is usual for a large σ parameter to contribute to the π parameter.

The phenolate oxygens are likely to have a large electrostatic contribution to the ligand field due to the negative charge localized on this atom. For example, a large electrostatic contribution has also been inferred for the phenolate oxygen in $Nd(Odpp)_3(thf)_2$ ($Odpp^- = 2,6$-diphenylphenolate).[35] Using a point charge electrostatic model with the geometry given in Table 1, the largest contribution of the phenolate O^- atoms is $B_{43} = 648 - i322$ cm^{-1}. We feel that the relatively small $e_\sigma(O)$ value found in Table 7 is a consequence of the neglect of the electrostatic contribution of the O^- atoms, rather than misdirected valence. However, it should be noted that the C5−O−Ln angle in the trensal complexes is much larger (~142°) than the 120° angle of sp^2 hybridization.

Conclusions

The B_{kq} parameters can be successfully expressed in a smaller number of AOM parameters if the *actual* geometry of the molecule is used rather than just the symmetry. The AOM parameters for different lanthanides could be related by assuming they are proportional to the eighth power of the bond length. This is due to the contraction of the f orbitals having a greater effect on the reduction of the metal−ligand overlap than the decreasing bond lengths have on increasing the metal−ligand overlap across the series. Anisotropic π-bonding parameters were required, and positive $e_{\pi\perp}$ values perpendicular to the pseudoaromatic bidentate rings indicated π donor properties of these atoms. The small value of $e_\sigma(O)$ is likely to be a consequence of neglecting the large electrostatic contribution to the ligand field expected for the charged coordinating atom of the phenolate group.

Acknowledgment. Financial support for this research was kindly provided by the University of Queensland. We gratefully acknowledge M. F. Reid for providing us with his computer programs.

Supporting Information Available: A text file containing the minor atomic parameters and the Fortran90 subroutine generated by Mathematica, giving the B_{kq} parameters in terms of the AOM parameters and the angle ϕ. This material is available free of charge via the Internet at http://pubs.acs.org.

IC011276Q

(31) Urland, W. *Chem. Phys. Lett.* **1981**, *83*, 116.
(32) Cruse, D. A.; Gerloch, M. *J. Chem. Soc., Dalton Trans.* **1977**, 152.
(33) Gerloch, M.; Hanton, L. R.; Manning, M. R. *Inorg. Chim. Acta* **1981**, *48*, 205.
(34) Gerloch, M. *Magnetism and Ligand Field Analysis*; Cambridge University Press: Cambridge, U.K., 1983.
(35) Deacon, G. B.; Feng, T.; Skelton, B. W.; White, A. H. *Aust. J. Chem.* **1995**, *48*, 741.